Journal of Alloys and Compounds 509 (2011) 5167–5172

Contents lists available at ScienceDirect

Journal of Alloys and Compounds

journal homepage: www.elsevier.com/locate/jallcom

X-ray diffraction and dielectric studies across morphotropic phase boundary in $(1-x)$ [$Pb(Mg_{0.5}W_{0.5})O_3$]–$xPbTiO_3$ ceramics

A.K. Singh, Akhilesh Kumar Singh*

School of Materials Science and Technology, Institute of Technology, Banaras Hindu University, Varanasi 221 005, India

ARTICLE INFO

Article history:
Received 4 August 2010
Received in revised form 3 February 2011
Accepted 5 February 2011
Available online 5 March 2011

Keywords:
PMW–*x*PT
Crystal structure
Morphotropic phase boundary
Dielectric
Phase diagram

ABSTRACT

We present here the results of comprehensive X-ray diffraction and dielectric studies on several compositions of $(1-x)$[$Pb(Mg_{0.5}W_{0.5})O_3$]–$xPbTiO_3$ (PMW–*x*PT) solid solution across the morphotropic phase boundary. Rietveld analysis of the powder X-ray diffraction data reveals cubic (space group *Fm*3*m*) structure of PMW–*x*PT ceramics for the compositions with $x \leq 0.42$, tetragonal (space group *P*4*mm*) structure for the compositions with $x \geq 0.72$ and coexistence of the tetragonal and cubic phases for the intermediate compositions ($0.46 \leq x \leq 0.68$). Temperature dependence of the dielectric permittivity above room temperature exhibits diffuse nature of phase transitions for the compositions in the cubic and two phase region while the compositions with tetragonal structure at room temperature exhibit sharp ferroelectric to paraelectric phase transition. The PMW–*x*PT compositions with coexistence of tetragonal and cubic phases at room temperature exhibit two anomalies in the temperature dependence of the dielectric permittivity above room temperature. Using results of structural and dielectric studies a partial phase diagram of PMW–*x*PT ceramics is also presented.

1. Introduction

In recent years there has been revival of interest in studying the electroceramics that exhibit morphotropic phase boundary (MPB) in their phase diagram [1,2]. The MPB was first discovered in $Pb(Zr_xTi_{1-x})O_3$ (PZT) ceramics, as the nearly temperature independent phase boundary that separates stability regions of tetragonal and rhombohedral (the actual structure is now known to be monoclinic) phases. The dielectric and piezoelectric response of the electroceramics exhibiting MPB such as PZT, $(1-x)Pb(Mg_{1/3}Nb_{2/3})O_3$–$xPbTiO_3$ (PMN–*x*PT) and $(1-x)Pb(Zn_{1/3}Nb_{2/3})O_3$–$xPbTiO_3$ (PZN–*x*PT) were found maximum near MPB [3]. The maximum electromechanical response near the MPB was earlier attributed to the coexistence of rhombohedral and tetragonal phases that makes available '14' polarization directions (6 for tetragonal along any of ⟨0 0 1⟩ and 8 for rhombohedral along any of ⟨1 1 1⟩ crystallographic directions). Recently it is shown that the structure of MPB indeed consists of coexistence of tetragonal and monoclinic phases in PZT [4], PMN–*x*PT [5], PZN–*x*PT [6], $(1-x)Pb(Fe_{1/2}Nb_{1/2})O_3$–$xPbTiO_3$ (PFN–*x*PT) [7] and $(1-x)Pb(Sc_{1/2}Nb_{1/2})O_3$–$xPbTiO_3$ (PSN–*x*PT) [8]. In monoclinic phase the polarization vector is not restricted to fixed crystallographic directions but have freedom to rotate in a plane [9]. The maximum dielectric and piezoelectric properties near the MPB makes it imperative to revisit the structure–property correlations in other MPB systems also.

The PMW–*x*PT ceramics belongs to the family of mixed perovskite relaxor–ferroelectric solid solutions. An early study on this system has been done by Krainik and Agranovskaya [10], and Smolenskii et al. [11] who reported that PMW–*x*PT with more than 10% PT shows hysteresis loop below the dielectric maximum. Further, they also reported that with increasing PT concentration for 0–10%, the Curie temperature decreases continuously and for higher PT concentrations ($x > 0.10$) it continuously increases. Yasuda et al. [12] have reported high dielectric constant (~15,000 at 100 kHz for $x = 0.58$ composition, at peak temperature (T_m)) and large spontaneous polarization ($P_s = 42\ \mu C/cm^2$ for $x = 0.60$) of PMW–*x*PT ceramics, which revealed that this material has potential for piezoelectric and pyroelectric applications. They have shown that the MPB between relaxor (pseudocubic) and normal ferroelectric (tetragonal) phases exist at $x = 0.58$ composition. In another study, Zaslavaskii and Bryzhina [13] reported that the pseudocubic to tetragonal phase transition occurs at $x = 0.45$. However, the structural studies by Yasuda et al. [12], revealed that the pseudocubic to tetragonal phase transition is observed around $x = 0.50$. In contrast, our recent investigation on this system shows that the composition dependence of the planar electromechanical coupling coefficient (k_P) shows a peak around $x = 0.68$ [14]. Thus the location of the MPB and structural studies on the MPB phases in PMW–*x*PT

* Corresponding author. Tel.: +91 542 2307047; fax: +91 542 2368707.
E-mail addresses: akhilesh_bhu@yahoo.com, akhilesh@bhu.ac.in, akhilesh_itbhu@rediffmail.com (A.K. Singh).

0925-8388/$ – see front matter © 2011 Elsevier B.V. All rights reserved.
doi:10.1016/j.jallcom.2011.02.027

ceramics is ambiguous and incomplete. There are few reports [15] where Rietveld structural analysis of the PMW is done but such a study has still not been done on PMW–*x*PT ceramics.

The present paper describes the precise location of MPB in PMW–*x*PT ceramics with detailed structural and dielectric characterization across the MPB region. Our detailed investigation of structure across MPB shows that, surprisingly, this system does not have any monoclinic phase in MPB region. The structure of the compositions in the MPB region is found to be coexistence of cubic (*Fm*3*m*) and tetragonal (*P*4*mm*) phases. In addition to this, we have observed two dielectric anomalies in the temperature dependence of the dielectric permittivity above room temperature, for the compositions lying in the two phase region, which was not reported previously for this system. Based on our detailed X-ray diffraction and dielectric studies we have reconstructed the phase diagram of PMW–*x*PT ceramics.

2. Experimental

PMW–*x*PT ceramics with compositions $x = 0.00, 0.42, 0.46, 0.50, 0.54, 0.58, 0.60, 0.64, 0.68, 0.72$ and 1.00 have been prepared by a modified solid state route. Details of the synthesis can be found elsewhere [14]. Analytical reagent (AR) grade H_2WO_4 (99%), TiO_2 (99%), $Mg(NO_3)_2{\cdot}3H_2O$ (99%), $Pb(NO_3)_2$ (99%), and ammonium carbonate were used for synthesis. Mixing of various ingredients in stoichiometric proportions was carried out for 6 h using a ball mill (Restch, Germany) with zirconia jars and zirconia balls. AR grade acetone was used as the mixing media. Heat treatment for calcination was carried out in alumina crucibles using a globar furnace. In the first step, the wolframite precursor $MgWO_4$ (MW) was prepared by calcining a stoichiometric mixture of $MgCO_3{\cdot}3H_2O$ and H_2WO_4 at 1000 °C for 6 h. At the next stage, stoichiometric amount of TiO_2 was mixed with $MgWO_4$ and the mixture was calcined at 1000 °C for 6 h to obtain $[(1-x)/2]MgWO_4$–$(x)TiO_2$ (MWT) precursor. This MWT precursor was then mixed with stoichiometric amount of $PbCO_3$ and calcined at 800 °C for 6 h to get PMW–*x*PT powders. Cold compaction of calcined powders was done using a uniaxial hydraulic press. Sintering of cold compacted disc pellets were carried out at 1100 °C for 6 h in controlled PbO atmosphere. The sintered pellets were crushed into fine powder which was annealed at 500 °C for 10 h for recording powder XRD data (compositions with lower PT concentration have some unidentified impurity whose fraction is very small (<1%)). For dielectric measurements, the flat surface of sintered pellets was gently polished with 0.25 μm diamond paste for about 2 min and then washed with acetone. Isopropyl alcohol was then applied to clean the surface for removing the moisture, if any, on the pellet surfaces. Fired on silver paste was subsequently applied on both the surface of the pellet. It was first dried around 120 °C in an oven and then cured by firing at 500 °C for about 5 min.

Powder X-ray diffraction patterns were recorded using an 18 kW rotating anode (Cu) based Rigaku powder diffractometer fitted with a graphite monochromator in the diffracted beam. FULLPROF program (Rodriguez-Carvajal [16]) was used for Rietveld refinement of the structure. Pseudo-Voight function was used to define the peak profiles and fifth-order polynomial was used to fit the background. Dielectric measurements were carried out using a Novocontrol, Alpha-A high performance frequency analyzer and a locally designed sample holder and furnace. The temperature of the sample was controlled by using a Eurotherm programmable temperature controller with an accuracy of ±1 °C. The measurements were carried out during heating the sample at a rate of 1 °C per min.

3. Results and discussion

3.1. X-ray diffraction studies on PMW–xPT ceramics

To analyse the room temperature structure of PMW–*x*PT ceramics we focused on some selected pseudocubic reflections whose profile splitting may help in determining the structure. Fig. 1 depicts the evolution of 100, 200, 220 and 222 pseudocubic reflections for various compositions of PMW–*x*PT ceramics. It is evident from Fig. 1 that for compositions with $x \geq 0.68$, diffraction profiles are similar to that for pure $PbTiO_3$. This suggests that the structure of PMW–*x*PT for compositions with $x > 0.68$ is tetragonal, as of $PbTiO_3$. The structure of pure PMW is known to be cubic in *Fm*3*m* space group above Curie temperature [15]. This is evident from Fig. 1, as all the profiles are seen to be singlet for $x = 0.00$. Similar to PMW, the pseudocubic reflections for the composition with $x = 0.42$ are singlet that suggests a cubic (*Fm*3*m*) structure for PMW–0.42PT also. For compositions with $0.46 \leq x \leq 0.64$, the

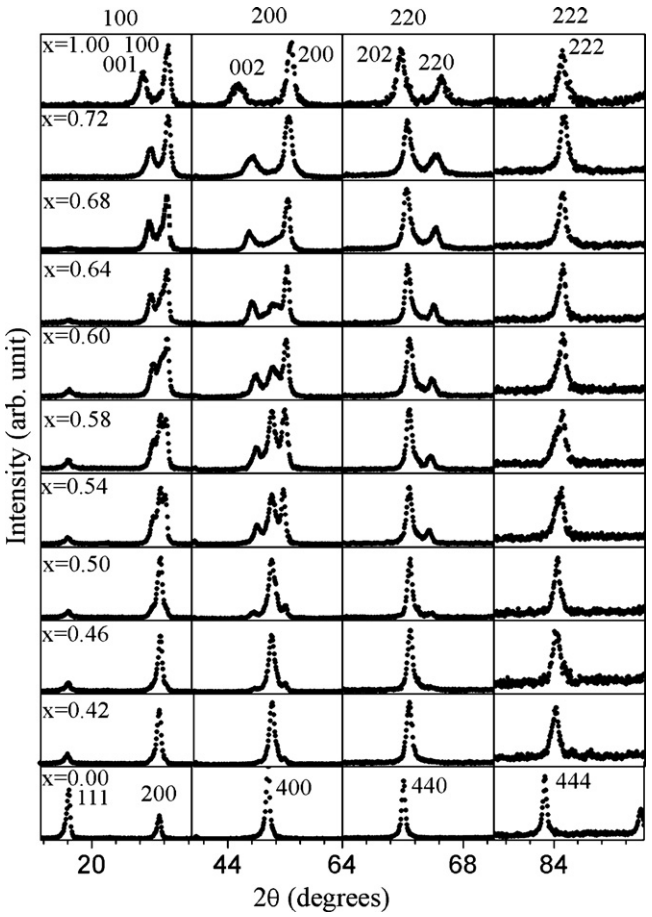

Fig. 1. Evolution of 100, 200, 220 and 222 pseudocubic reflections of PMW–*x*PT ceramics with composition. The indices shown above the diffraction peaks for $x = 1.00$ correspond to tetragonal (space group *P*4*mm*) unit cell while for $x = 0.00$ correspond to cubic (space group *Fm*3*m*) unit cell.

coexistence of tetragonal (*P*4*mm*) and cubic (*Fm*3*m*) structures is observed as is evident from the triplet nature of the diffraction profile around $2\theta = 45.5°$. Because of the proximity of lattice parameters of tetragonal (*P*4*mm*) and cubic (*Fm*3*m*) structures, their diffraction lines partially overlap in the coexistence region. The central peak corresponds to the cubic (*Fm*3*m*) (4 0 0) reflection and the extreme ones are the tetragonal (*P*4*mm*) (0 0 2) and (2 0 0) Bragg reflections, respectively. The intensity of central (4 0 0) peak corresponding to cubic (*Fm*3*m*) phase gradually decreases with increasing '*x*' in the coexistence region. This suggests that the fraction of cubic (*Fm*3*m*) phase decreases with increasing PT concentration. In addition to this, with increasing '*x*' the intensity of the superlattice reflection at $2\theta \approx 19.22$ (Miller indices are 1/2, 1/2, 1/2 when indexed with respect to pseudocubic cell) which appear due to 1:1 ordering of B-site Mg^{2+}/W^{6+} cations [15] decreases. Thus the substitution of Ti^{4+} at Mg^{2+}/W^{6+} site tends to decrease the cationic ordering in favor of disordered solid solution.

We carried out Rietveld analysis of the powder X-ray diffraction data of all the compositions of PMW–*x*PT ceramics prepared in the present work to confirm unambiguously the structures discussed above. The Rietveld analysis of XRD data confirms that PMW–*x*PT ceramics with compositions $x \geq 0.72$ exhibit single phase tetragonal structure with space group *P*4*mm*. Very good fit between observed and calculated profiles obtained for the composition with $x = 0.72$ using tetragonal (*P*4*mm*) structure is illustrated in Fig. 2. Rietveld analysis of the X-ray diffraction data for $x = 0.68$ reveals small fraction of coexisting cubic (*Fm*3*m*) phase along with the majority tetragonal phase. Since the diffraction profiles are singlet in the

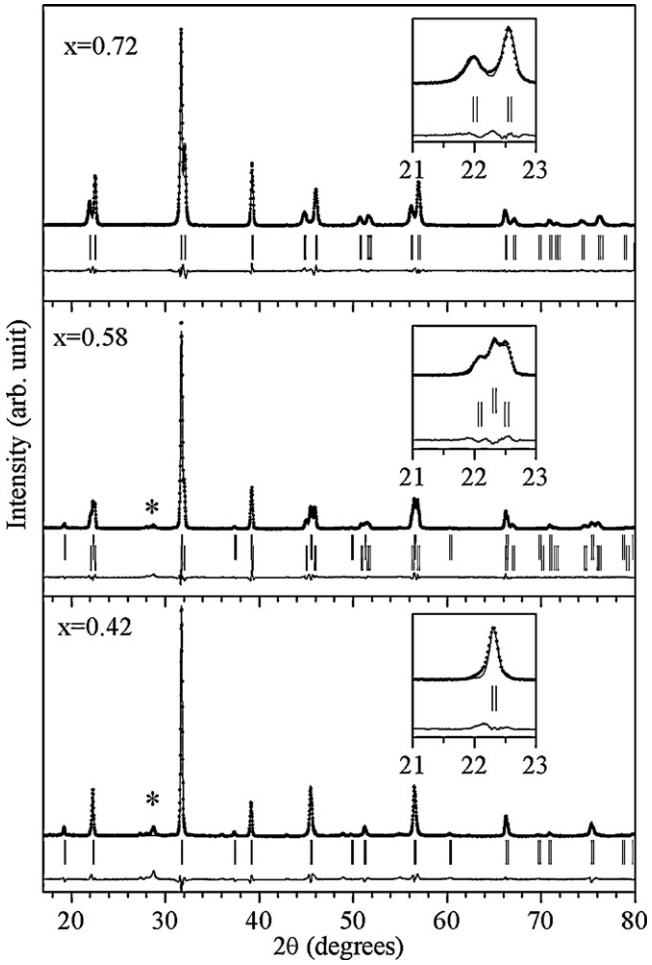

Fig. 2. Observed (dots), calculated (continuous line), and difference (bottom line) profiles obtained after the Rietveld refinement of the structure of PMW–*x*PT for $x = 0.42$, 0.58 and 0.72 using cubic (space group *Fm*3*m*), cubic + tetragonal (space group *Fm*3*m* + *P*4*mm*) and tetragonal (*P*4*mm*) phases, respectively. The inset illustrates the quality of fit for the pseudocubic 100 profile. The tick marks above the difference plot show the positions of the Bragg peaks. In PMW–0.58PT composition, lower and upper tick marks are for tetragonal and cubic phases, respectively. The peak ($\sim 2\theta = 28.54$) marked with asterisk is unidentified impurity whose fraction is very small (<1%).

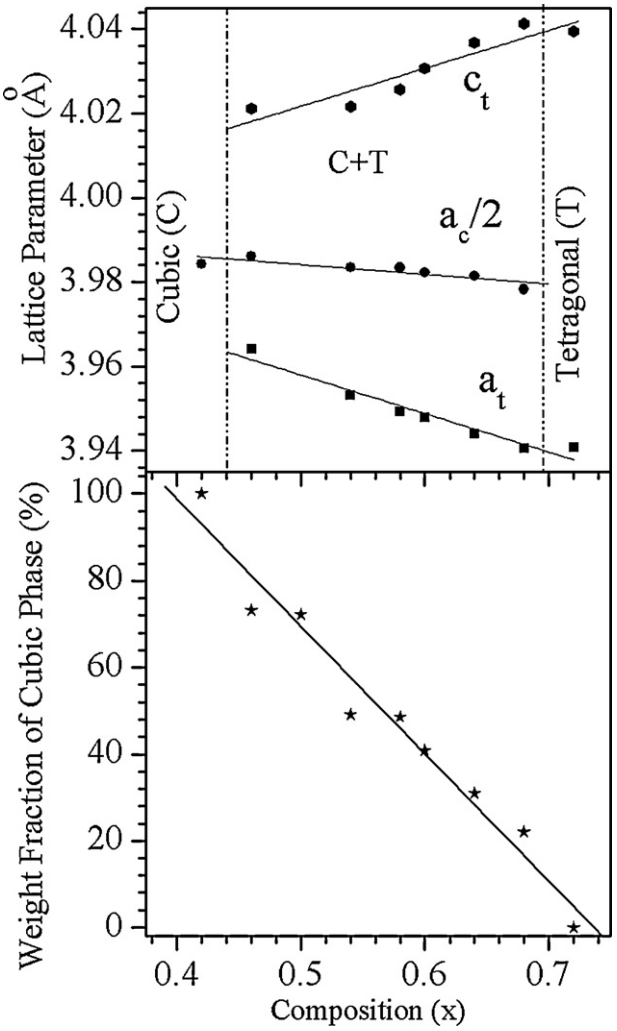

Fig. 3. Variation of (a) lattice parameters (b) weight fraction of cubic phase, with composition for PMW–*x*PT ceramics.

composition range $0.00 \le x \le 0.42$, we considered cubic *Fm*3*m* space group for refining the structure in this composition range. For completeness we have also considered the orthorhombic *Pmcn* (*Pnma*) space group of antiferroelectric phase of PMW reported below room temperature [15]. Consideration of *Pmcn* space group did not result a good fit between observed and calculated patterns. The best fit was obtained for cubic phase in *Fm*3*m* space group (see the fit in Fig. 2 for $x = 0.42$) which was earlier reported by Baldinozzi et al. [15] for PMW above Curie temperature. The structure of PMW–*x*PT ceramics in the composition range $0.46 \le x \le 0.68$ were refined well by considering the coexistence of tetragonal (*P*4*mm*) and cubic (*Fm*3*m*) phases. Very good fit between observed and calculated patterns is obtained by considering coexistence of tetragonal and cubic phases for the composition range $0.46 \le x \le 0.68$. This is illustrated in Fig. 2 for PMW–0.58PT. In view of the discovery of new monoclinic phases in the phase coexistence region of other MPB ceramics like PZT, PMN–*x*PT, PZN–*x*PT etc. [4–8], we also considered various low symmetry structures for refining the structure of PMW–*x*PT ceramics in the composition range $0.46 \le x \le 0.68$. We did not find any new structure for this composition range. There is indeed the coexistence of tetragonal and cubic phases.

In an earlier study, Zaslavaskii and Bryzhina [13] has reported that the structure of PMW–*x*PT ceramics is cubic for $x \le 0.45$ and tetragonal for $x > 0.45$. Yasuda et al. [12] reported that PMW–*x*PT has pseudocubic structure for $x = 0.4$ and it begins to show tetragonal distortion around $x = 0.5$. However, these workers could not detect any phase coexistence region possibly due to low intensity XRD data with poorer resolution. Our XRD data has been recorded on 18 kW rotating anode XRD machine. Similar to our finding coexistence of tetragonal and cubic phase has been observed in MPB region of PFW–*x*PT ceramics also (Mistoseriu et al. [17]). However, in case of PFW–*x*PT ceramics the space group of cubic phase is *Pm*3*m* and not *Fm*3*m*.

Fig. 3(a) depicts the variation of the lattice parameters with composition. For easy comparison of the lattice parameter of cubic (*Fm*3*m*) phase with tetragonal (*P*4*mm*) phase, we have divided the lattice parameter of cubic phase by 2. It is evident form Fig. 3(a) that the cubic cell parameter a_c decreases linearly with increasing PT content. The c_t parameter of tetragonal phase increases continuously with increasing PT content while a_t parameter decreases. As expected, the tetragonality of PMW–*x*PT ceramics increases linearly with increasing PT concentration. Fig. 3(b) depicts the variation of the weight fraction of cubic (*Fm*3*m*) phase with composition. For the compositions with $x \le 0.42$ structure is pure cubic in *Fm*3*m* space group while it is pure tetragonal for compositions with $x \ge 0.72$ (see Table 1). The two phases coexist for intermediate

Table 1
Variation of cubic phase fraction and lattice parameter with composition in PMW–*x*PT ceramics.

Composition (x)	Weight fraction of cubic phase (%)	Lattice parameters		
		Cubic phase	Tetragonal phase	
		$a_C/2$ (Å)	a_t (Å)	c_t (Å)
0.00	100.00	4.002 (1)	–	–
0.42	100.00	3.9838 (1)	–	–
0.46	73 (1)	3.9861 (1)	3.9640 (3)	4.0211 (2)
0.50	72.2 (6)	3.9833 (1)	3.9527 (2)	4.0260 (2)
0.54	49.5 (8)	3.9828 (3)	3.95277 (2)	4.0202 (3)
0.58	47.5 (6)	3.9832 (2)	3.94928 (8)	4.02574 (1)
0.60	40.8 (6)	3.9822 (3)	3.94800 (8)	4.0306 (1)
0.64	31.0 (4)	3.9814 (3)	3.94407 (7)	4.0367 (1)
0.68	22.1 (4)	3.9783 (3)	3.9406 (7)	4.0413 (1)
0.72	0.00	–	3.9411 (1)	4.0395 (1)
1.00	0.00	–	3.904	4.150

compositions. The weight fraction of cubic phase linearly decreases with increasing PT concentration in PMW–*x*PT ceramics.

3.2. Dielectric studies

In an early study, Yasuda et al. [12] have reported that the temperature dependence of dielectric permittivity in PMW–*x*PT ceramics exhibit relaxor like features for the compositions with $x = 0.50$ and 0.55. To investigate the nature of phase transitions in PMW–*x*PT ceramics, we have carried out temperature dependent dielectric studies on several compositions ($x = 0.42$, 0.46, 0.50, 0.58, 0.60, 0.68 and 0.72) lying in the cubic, phase coexistence and tetragonal phase regions at room temperature. Fig. 4 shows the temperature dependence of the dielectric permittivity for $x = 0.42$, 0.46, 0.50, and 0.68, respectively, at various measuring frequencies. It is evident from this figure that for all the compositions there is no visible frequency dependent shift in the temperature at which dielectric constant shows a peak. However, the dielectric permittivity peaks are significantly broad which indicates diffuse nature of these phase transitions. It is clearly seen in Fig. 4, that the composition with $x = 0.50$ exhibit two dielectric anomalies above room temperature, first at 104 °C and second at 180 °C. Similarly the composition with $x = 0.46$ also exhibit two overlapping dielectric anomalies above room temperature at 92 °C and 152 °C. We observed that all the compositions that show phase coexistence at room temperature exhibit two dielectric anomalies in the temperature dependence of the dielectric permittivity above room temperature. For lower PT concentration the first dielectric anomaly is stronger than the second one appearing on higher temperature such as for ($x = 0.46$). With increasing PT concentration and consequent increase in the phase fraction of tetragonal phases, the dielectric anomaly appearing on higher temperatures becomes stronger in magnitude in comparison to that at the lower temperatures as seen in Fig. 4 for $x = 0.50$. At further higher PT concentration, the dielectric anomaly on the lower temperature side weakens and disappears in the pure tetragonal phase region. As shown in Fig. 4 for $x = 0.68$, the first dielectric anomaly appearing on the lower temperature side is barely visible in the real part of dielectric permittivity and can be seen only in imaginary part. Similarly, the second dielectric anomaly appearing on the higher temperature side weakens with decreasing PT concentration and disappears for the single phase cubic ($Fm3m$) region. Thus, the composition with $x = 0.42$ (cubic) exhibit only one dielectric peak at 78 °C and the composition with $x = 0.72$ (tetragonal) exhibit only one dielectric peak at 288 °C (not shown here). In contrast to the present work, Yasuda et al. [12] and, Krainik and Agranovskaya [10] have reported only one dielectric anomaly for the compositions in the MPB region also. It will be interesting to investigate in future the origin of the two dielectric anomalies in the phase coexistence region and also their correlation with the phase fraction of the cubic and tetragonal phases as discussed above.

As stated earlier, the dielectric anomalies for all the four compositions shown in Fig. 4 exhibit very diffuse peak like relaxor ferroelectrics but the temperature of dielectric permittivity maximum is independent of frequency like in normal ferroelectrics.

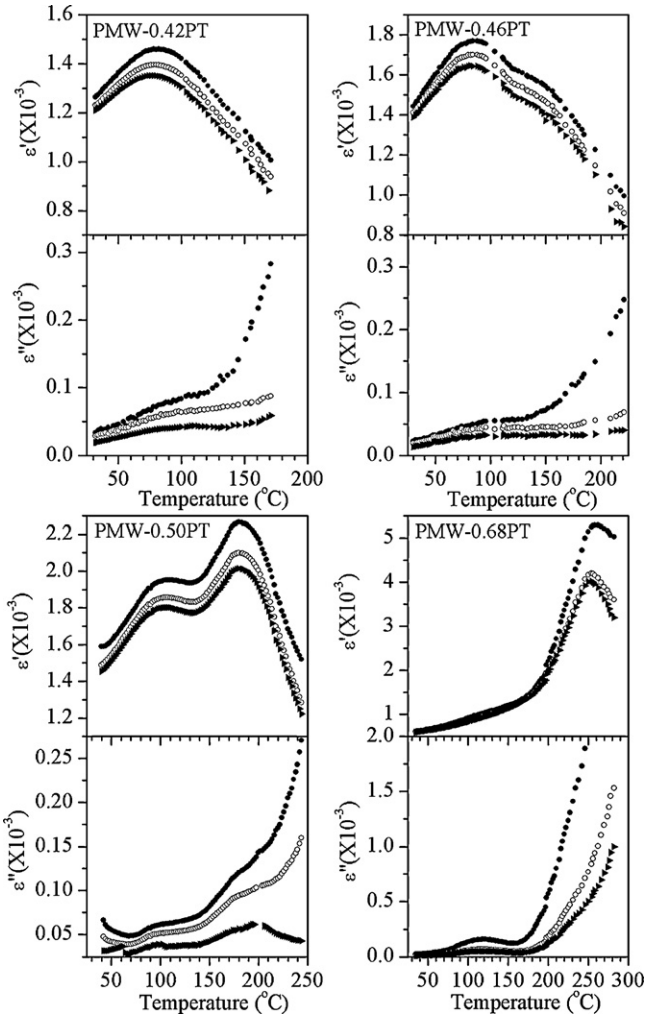

Fig. 4. Temperature dependence of dielectric permittivity of PMW–*x*PT ceramics for $x = 0.42$, 0.46, 0.50 and 0.68 compositions, measured at 1 kHz (solid dots), 10 kHz (open circle) and 100 kHz (triangle).

Similar behaviour in the temperature dependence of dielectric permittivity has been seen in some other solid solutions also [18–20]. It is proposed that the diffuse phase transition behaviour is intermediate between relaxor and normal ferroelectric phase transitions. Particularly in $Ba(Ti_{1-x}Sn_x)O_3$, it has been shown that the normal ferroelectric phase transition behaviour of $BaTiO_3$ changes to relaxor behaviour showing significant frequency dependent shift in the peak temperature of dielectric permittivity for the composition with $x = 0.30$, whereas the composition with $x = 0.20$ exhibit diffuse peak in dielectric permittivity which is independent of frequency. Thus phase transition changes from normal ferroelectric type (pure $BaTiO_3$) to diffuse phase transition ($x = 0.20$) to relaxor behaviour ($x = 0.30$) by increasing disorder at B-site introduced by substituting Ti^{4+} by Sn^{4+}. Hence it may be concluded that the PMW–*x*PT ceramics studied in the present work exhibit diffuse phase transition behaviour intermediate between normal and relaxor behaviour. It is important to mention here that the nature of phase transition is also associated with the B-site cationic ordering. It was reported by Setter and Cross [21] that degree of ordering of B-site cations has strong influence on the nature of phase transition in $Pb(Sc_{0.5}Ta_{0.5})O_3$ ceramics. The sample in which B-site cations are disordered exhibit diffuse phase transition while normal first order ferroelectric phase transition is observed in the samples which were annealed for long duration that induces ordering of the B-site (Sc^{3+}/Ta^{5+}) cations. Thus increasing the degree of ordering on B-site cations sharpens the diffuse transition. The small frequency dependent shift in the peak temperature of dielectric permittivity reported by Yasuda et al. [12] in PMW–*x*PT ceramics for the compositions with $x = 0.50$ and 0.55 may be due to higher disorder of cations at B-site in their samples. Recently Hong et al. [22] have shown that sintering temperature of the samples also affect the nature of phase transition, and relaxor like phase transition behaviour to normal ferroelectric phase transition behaviour may be observed in sample of same composition by changing the sintering temperature that possibly affects the disorder of B-site cations. The degree of ordering of cations at B-site in our samples (sintered at 1100 °C) might be different from the samples of Yasuda et al. [12] which was sintered at 1050 °C. This may be the reason why we do not observe any obvious frequency dependent shift in the peak temperature of the dielectric permittivity.

At this stage it is not clear to us that the two permittivity peaks observed for the compositions in the phase coexistence region ($0.46 \le x \le 0.68$) shown in Fig. 4 are due to structural phase transitions or one anomaly is due to structural phase transition and the other one is due to dielectric relaxation, or both the peaks solely have their origin in dielectric relaxation as is the case with canonical relaxor ferroelectric PMN [23]. A detailed high temperature diffraction study in conjunction with dielectric studies will be needed to settle the origin of the dielectric anomalies and the nature of phase transition observed in PMW–*x*PT ceramics.

3.3. Partial phase diagram of PMW–xPT ceramics

Fig. 5 shows the partial phase diagram of PMW–*x*PT ceramics established on the basis of new findings in this work. The transition/dielectric anomaly temperature reported by Yasuda et al. [12] is also included in this figure and is shown by open circles. The dotted vertical line shown in Fig. 5 around the composition with $x \approx 0.43$ separates the stability fields of the cubic ($Fm3m$) and phase coexistence ($Fm3m + P4mm$) regions while the dotted vertical line around the composition with $x \approx 0.68$ separates the stability fields of phase coexistence ($Fm3m + P4mm$) and tetragonal ($P4mm$) phase regions. The structure of the tetragonal compositions ($x \ge 0.72$) above the dielectric anomaly temperature is expected to be cubic in the $Pm3m$ space group similar to that for pure $PbTiO_3$, as no cationic ordering at B-site is seen at room temperature for these compositions. The structure of the high temperature phases for the compositions in cubic ($Fm3m$) and phase coexistence ($Fm3m + P4mm$) regions is not known and is subject matter of future investigations. The two anomalies in the temperature dependence of dielectric permittivity above room temperature for the compositions in the two phase region points towards another unknown region in the phase diagram of PMW–*x*PT ceramics. High temperature X-ray diffraction studies of various compositions of the PMW–*x*PT ceramics are underway and the structure of these unknown phases will be reported separately.

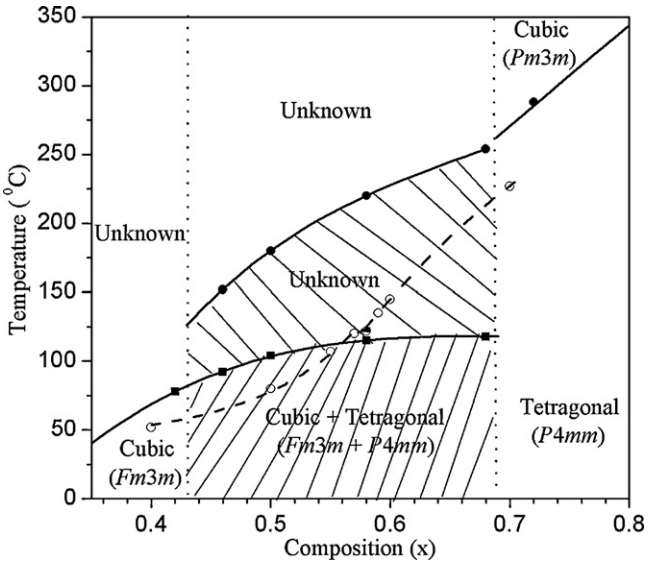

Fig. 5. Phase diagram of PMW–*x*PT ceramics. The transition/dielectric maximum temperature reported by Yasuda et al. [10] is shown by open circle. The continuous lines are guide to eye.

4. Conclusion

Rietveld analysis of the room temperature powder X-ray diffraction data on several compositions of PMW–*x*PT ceramics across the morphotropic phase boundary reveals cubic (space group $Fm3m$) structure for the compositions with $x \le 0.42$, tetragonal (space group $P4mm$) structure for the compositions with $x \ge 0.72$ and coexistence of the tetragonal and cubic phases for the intermediate compositions ($0.46 \le x \le 0.68$). The PMW–*x*PT compositions with the coexistence of tetragonal and cubic phases at room temperature exhibit two anomalies in the temperature dependence of the dielectric permittivity above room temperature which was not reported previously for this system. Based on our detailed X-ray diffraction and dielectric studies we have reconstructed the phase diagram of PMW–*x*PT ceramics. Our investigation on PMW–*x*PT ceramics calls for more work to be carried out in future to understand the structural phases and nature of phase transitions present in this system.

Acknowledgements

Authors are thankful to Professor Dhananjai Pandey, School of Materials Science and Technology, IT, BHU, Varanasi, India for extending laboratory facilities. Mr. A.K. Singh acknowledges CSIR, India for providing financial assistance in the form of SRF.

References

[1] D. Pandey, A.K. Singh, S. Baik, Acta Crystallogr. A64 (2008) 192.
[2] B. Noheda, D.E. Cox, Phase Transitions 79 (2006) 5.

[3] B. Jaffe, W.R. Cook, H. Jaffe, Piezoelectric Ceramics, Academic Press, London, 1971.
[4] B. Noheda, D.E. Cox, G. Shirane, R. Guo, B. Jones, L.E. Cross, Phys. Rev. B 63 (2000) 014103;
Ragini, R. Ranjan, S.K. Mishra, D. Pandey, J Appl. Phys. 92 (2002) 3266;
D. Pandey, A.K. Singh, R. Ranjan, Ragini, Ferroelectrics 325 (2005) 35;
A.K. Singh, D. Pandey, S. Yoon, S. Baik, N. Shin, Appl. Phys. Lett. 91 (2007) 192904.
[5] A.K. Singh, D. Pandey, J. Phys.: Condens. Matter 13 (2001) L931;
A.K. Singh, D. Pandey, Phys. Rev. B 67 (2003) 064102;
A.K. Singh, D. Pandey, Ferroelectrics 326 (2005) 91;
A.K. Singh, D. Pandey, O. Zaharko, Phys. Rev. B 74 (2006) 024101.
[6] J.M. Kiat, Y. Uesu, B. Dkhil, M. Matsuda, C. Malibert, G. Calvarin, Phys. Rev. B 65 (2002) 064106.
[7] S.P. Singh, A.K. Singh, D. Pandey, J. Phys.: Condens. Matter 19 (2007) 036217.
[8] R. Haumont, A. Al-Barakaty, B. Dkhil, J.M. Kiat, L. Bellaiche, Phys. Rev. B 71 (2005) 104106.
[9] H. Fu, R.E. Cohen, Nature 403 (2000) 281.
[10] N.N. Krainik, A.I. Agranovskaya, Sov. Phys. Solid State 2 (1960) 63.
[11] G.A. Smolenskii, N.N. Krainik, A.I. Agranovskaya, Sov. Phys. Solid State 3 (1961) 714.
[12] N. Yasuda, H. Tauchi, K. Ohki, K. Uchino, J. Kor. Phy. Soc. 32 (1998) 1024.
[13] A.I. Zaslavaskii, M.F. Bryzhina, Sov. Phys. Crystallogr. 7 (1963) 5.
[14] A.K. Singh, A.K. Singh, Integr. Ferroelectr. 117 (2010) 129.
[15] G. Baldinozzi, P. Sciau, Acta Crystallogr. B51 (1995) 668;
K.Z. Baba-Kishi, G. Cressey, R.J. Cernik, J. Appl. Crystallogr. 25 (1992) 477;
A.K. Singh, A.K. Singh, Sol. State Sci. (to be published).
[16] J. Rodriguez-Carvajal, FULLPROF, Laboratory Leon Brillouin (CEA-CNRS) CEA/Saclay, 91191 Gif sur Yvette Cedex, France, 2007.
[17] L. Mistoseriu, P.M. Vilarinnho, J.L. Baptista, Appl. Phys. Lett. 80 (2002) 4422.
[18] V.V. Shvartsman, W. Kleemann, J. Dec, Z.K. Xu, S.G. Lu, J Appl. Phys. 99 (2006) 124111.
[19] I. Rivera, A. Kumar, N. Ortega, R.S. Katiyar, S. Lushnikov, Solid State Commun. 149 (2009) 172.
[20] C.R. Zhou, X.Y. Liu, W.Z. Li, C.L. Yuan, Solid State Commun. 149 (2009) 481.
[21] N. Setter, L.E. Cross, J. Appl. Phys. 51 (1980) 4356.
[22] C.H. Hong, S.Y. Chu, C.H. Hsu, J. Appl. Phys. 107 (2010) 094110.
[23] Z.Y. Cheng, R.S. Katiyar, X. Yao, A. Guo, Phys. Rev. B 55 (1997) 8165.